Evidence of magnetization switching by anomalous spin Hall torque in NiFe

T. Y. Ma [1,2,*] C. H. Wan,[1,*] X. Wang,[1] W. L. Yang,[1] C. Y. Guo,[1] C. Fang,[1] M. K. Zhao,[1] J. Dong,[1] Y. Zhang [1]
and X. F. Han [1,2,3,†]

[1]*Beijing National Laboratory for Condensed Matter Physics, Institute of Physics, University of Chinese Academy of Sciences,
Chinese Academy of Sciences, Beijing 100190, China*
[2]*Center of Materials Science and Optoelectronics Engineering, University of Chinese Academy of Sciences, Beijing 100049, China*
[3]*Songshan Lake Materials Laboratory, Dongguan, Guangdong 523808, China*

Recently the anomalous Hall effect was predicted as a possible mechanism to produce magnetization-dependent spin current. Here we have applied NiFe/Ru/perpendicular magnetic multilayers and a specific geometry to demonstrate magnetization switching driven by anomalous spin-orbit torque resulting from the bulk anomalous Hall effect. The anomalous spin Hall torque of NiFe is strong enough not only to switch the magnetization of perpendicular Co but also leads to opposite switching chirality compared with the ordinary spin Hall torque. This work confirmed the existence of a strong anomalous spin Hall torque due to anomalous Hall effect, which may lay a foundation to develop spin-orbit torque devices free of heavy metals.

I. INTRODUCTION

Spin-orbit torques (SOTs) provide a fast and energy-efficient way to switch magnetization [1–3] and have attractive potential in magnetic random access memory (MRAM) and spin logic applications [4–6]. The SOT can be easily observed in heavy metal/ferromagnetic metal (HM/FM) bilayers and normally originates from spin Hall effect and Rashba effect [7,8]. For the spin Hall origin, current J_c flowing through a heavy metal can generate a spin current $\sigma_{SHE} \propto \theta_{SHE}(n \times J_c)$, with n and θ_{SHE} being film normal and spin Hall angle, respectively. Then the spin current is absorbed by the ferromagnetic metal. Simultaneously the angular momentum carried by the spin current is also transferred to the FM layer in the form of dampinglike torque ($m \times \sigma_{SHE} \times m$) or fieldlike torque ($m \times \sigma_{SHE}$) [9]. Efficient spin sources are normally served by heavy metals with sizable spin-orbit coupling strength such as Pt [3,10], Pt-based alloys [11], Ta [2,10,12], W [13], Pd [14], PtMn [15], and IrMn [16,17], or topologic insulators with spin-momentum locked surface states such as Bi_2Se_3 and $Bi_2(Se_{1-x}Te_x)_3$ [18]. In all the above cases, the polarization of σ_{SHE} constrained by the geometry of the current channel cannot be altered.

Spin current can also be obtained in magnetic materials. Besides the ordinary geometry-constrained spin current, magnetic materials can also give birth to magnetization-dependent spin current components with high efficiency, which grants us a flexible manner to produce polarization-tunable SOT. In theory, the anomalous Hall effect (AHE) and planar Hall effect (PHE) [19] inside magnetic materials or interfacial spin-related scattering [20] on the interface of magnetic

materials with nonmagnetic materials can produce spin current. Specifically, AHE, though discovered one century ago, is just recently predicted as a probable spin current source [19,21]. When m and J_c are noncollinear, spin-polarized electrons can be scattered into the transverse direction via $m \times J_c$ owing to the spin-orbit coupling, which gives rise to the anomalous Hall voltage as well as a pure spin current with polarization parallel with m. After its electric cousin AHE, this effect is renamed the anomalous spin Hall effect (ASHE).

In experiments, Safranski *et al.* [22] tried spin torque–ferromagnetic resonance to confirm PHE-originated SOT. Das *et al.* demonstrated the efficiency of AHE in generating spin current via magnon-mediate current-drag effect [23]. Furthermore, SOT switching was realized for in-plane NiFe/Ti/perpendicular CoFeB trilayer with T-type magnetic anisotropy, which was attributed to the interfacial spin-precessional scattering [24] on the NiFe and Ti interface. Magnetization switching driven by current was also reported in in-plane CoFeB/Mo/perpendicular CoFeB trilayer [25]. However, only ordinary magnetization-independent SHE torque of CoFeB was demonstrated in this reference. Recently, Seki *et al.* [26] reported that the SOT generated by ASHE of FePt could switch magnetization of NiFe with in-plane anisotropy, and Gibbons *et al.* [27] discussed ASHE-torque calibration using the second-harmonic Hall method. But SOT originating from the bulk AHE of a magnetic material as well as its SOT switching of perpendicular magnetization is still to be investigated and realized.

In this paper, we also used a core structure of NiFe/Ru/perpendicular ferromagnetic trilayer but a specific geometry to verify the bulk ASHE torque. In this geometry, pinned magnetization of NiFe (M_{NiFe}) by exchange bias, applied current parallel with M_{NiFe}, and applied field H_x transverse to M_{NiFe} was critical to achieve our targeted goal as discussed below. Our results demonstrated that the ASHE torque of NiFe

---

*These authors contributed equally to this work.
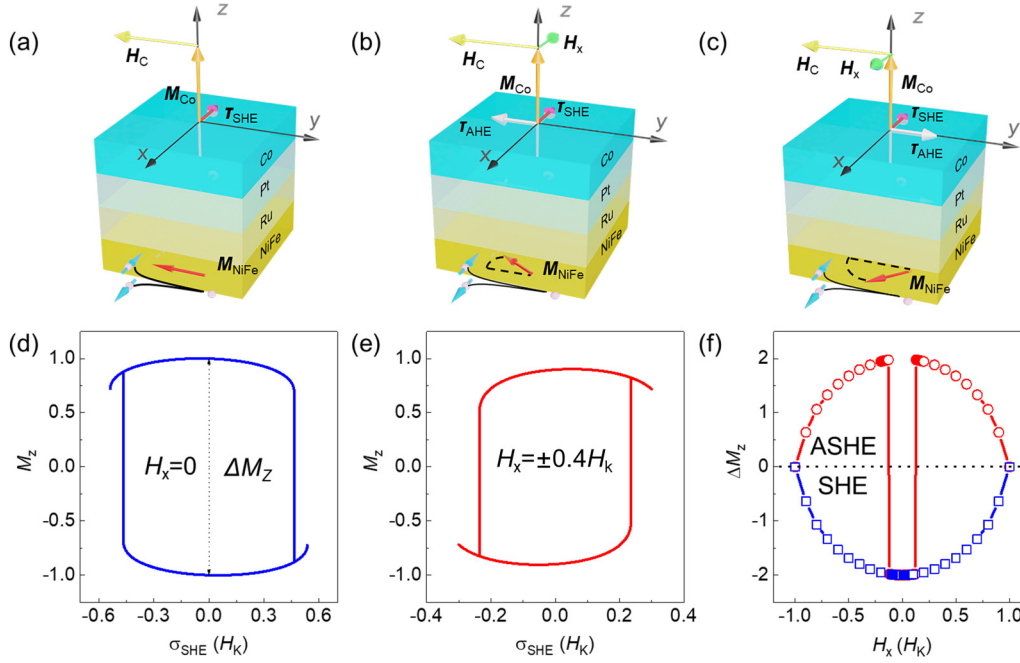†Corresponding author: xfhan@iphy.ac.cn

FIG. 1. Schematic diagrams of SOT switching driven by (a) the ordinary SHE and by interplay of the ordinary and anomalous SHE under (b) a small negative or (c) a small positive H_x. $\tau_{\text{SHE(AHE)}} = M_{\text{Co}} \times \sigma_{\text{SHE(AHE)}} \times M_{\text{Co}}$. H_x tilts M_{NiFe} away from the direction of applied current, which enables an anomalous Hall effect to occur via $M_{\text{NiFe}} \times J_c$. Calculated dependence of M_z on current or torque in units of H_K with (d) $H_x = 0$ and (e) $H_x = \pm 0.4 H_K$. (f) ΔM_z (torque=0) chirality as a function of H_x. Note that after anomalous SHE is taken into account, the switching chirality can be switched from -1 (CW) to $+1$ (CCW). Otherwise, ordinary SHE can only produce the -1 chirality. Calculation was based on the following parameters $H_C = 0.05 H_K$ and $H_{\text{EB}} = 0.3 H_K$.

could be not only strong enough to switch magnetization but also lead to opposite switching chirality with ordinary SHE-torque switching. Therefore this work experimentally verified the newly predicted ASHE torque due to the century-old AHE mechanism not only exists but is also strong, which might lay a foundation for the development of heavy-metal-free SOT devices.

II. EXPERIMENTS

The stack SiO_2//Ta(2)/IrMn(8)/NiFe($t_{\text{NiFe}} = 1, 3, 5$)/Ru (2)/Pt(1)/Co(1)/Pt(1 nm) was deposited by a magnetron sputtering system (ULVAC) with a base pressure of 1.0×10^{-6} Pa. The sputtering system was equipped with a magnetic field of 300 Oe to induce an easy axis during growth. The obtained NiFe in the full stack had an easy axis along the y direction, while the Co sandwiched by the two Pt layers had perpendicular magnetic anisotropy (PMA). Another SiO_2//Ru(2)/Pt(1)/Co(1)/Pt(1 nm) film was deposited as a control stack. A vibrating sample magnetometer (VSM, Microsense) was used to measure the hystereses of the stacks. We then patterned the stacks via ultraviolet lithography and subsequent argon ion etching technique into crossbar devices with width (length) of 20 μm (200 μm). Pt(5)/Au(80 nm) pads were used to connect the crossbar terminals. A Keithley 2400 (2182) source meter was used to provide the source current (pick up the Hall voltage). A physical property measurement system and an electromagnetic probe workstation were used to provide magnetic fields during transport and switching experiments. The electromagnetic probe

workstation was equipped with three-dimensional Helmholtz coils without iron cores, which makes its maximum magnetic field reach 340 Oe and resolution better than 0.05 Oe. All the measurements were conducted at room temperature.

III. RESULTS AND DISCUSSION

Figure 1 shows how SHE or ASHE torques switch perpendicular magnetization. In Fig. 1(a), M_{NiFe} was pinned along the y direction by an exchange bias field H_{EB} or $\varphi_{\text{NiFe}} = 270°$. The θ and φ denoted polar angle and azimuth angle, respectively. Then the coupling field H_C between NiFe and Co was also parallel with the y axis. Current J_c applied in the y direction produced spin current σ_{SHE} via ordinary SHE [28]. The σ_{SHE} was polarized in the x axis. The parallel relation between M_{NiFe} and J_c made AHE absent in this case. In this work, the direction of σ denotes the spin-polarization direction of spin current and the absolute value of σ denotes the magnitude of spin current density in magnetic field units. Notice that the spin current density $J_s = (\hbar/2e)\theta_{\text{SHE}}J_c$ and the dampinglike field $H_{\text{DL}} = \hbar\theta_{\text{SHE}}J_c/(2\mu_0 e M_s t) = J_s/(\mu_0 M_s t)$. In this paper, we actually used $\sigma_{\text{SHE}} = H_{\text{DL}} = J_s/(\mu_0 M_s t)$ to characterize the magnitude of J_s for simplicity, since spin current density was proportional to the dampinglike field. They were different only by a constant coefficient $1/(\mu_0 M_s t)$. Here, M_S was saturated magnetization, t was the thickness of the perpendicular layer, $\hbar$ was the reduced Planck constant, θ_{SHE} was the spin Hall angle, μ_0 was the permeability of vacuum, and J_c was the current density. The flow of the spin current is always along the z direction, since the free layer Pt/Co/Pt

sandwich is on top of the spin current generator NiFe. Then at the steady state, torque produced by the effective field H_{eff} should be balanced by the transferred spin-orbit torque induced by σ_{SHE} or $m_{\text{Co}} \times H_{\text{eff}} + m_{\text{Co}} \times \sigma_{\text{SHE}} \times m_{\text{Co}} = 0$. H_{eff} was determined by perpendicular anisotropic energy E_K, the coupling field H_C with NiFe and Zeeman splitting induced by the applied field H_x if any. According to a type-Z scheme [29], the perpendicular Co could be switched owing to the orthogonal configuration among σ_{SHE}, H_C, and easy axis (EA) of Co. The above torque equilibrium condition could be simplified as Eq. (1), as $H_x = 0$, similar to Ref. [3]. The terms in the left-hand side of Eq. (1) denoted torques induced by the anisotropic field H_K, the coupling field H_C, and the applied SHE torque σ_{SHE}. $H_K = 2E_K/M_S$. E_K and M_S were perpendicular anisotropic energy and saturated magnetization of the Co layer, respectively. This equation could generate a M_z vs σ_{SHE} curve in Fig. 1(d):

$$H_K \sin\theta \cos\theta + H_C \cos\theta - \sigma_{\text{SHE}} = 0. \quad (1)$$

After H_x was applied, M_{NiFe} was tilted away from the y direction or $\varphi_{\text{NiFe}} \neq 270°$. Due to the nonvanishing $M_{\text{NiFe}} \times J_c$ term, AHE occurred. Because of this AHE mechanism, a pure spin current σ_{AHE} parallel with M_{NiFe} was also produced. Taking this additional ASHE torque into account, the torque equilibrium equation was reformed as $m_{\text{Co}} \times H_{\text{eff}} + m_{\text{Co}} \times \sigma_{\text{SHE}} \times m_{\text{Co}} + m_{\text{Co}} \times \sigma_{\text{AHE}} \times m_{\text{Co}} = 0$, or equivalently, Eq. (2):

$$H_K \sin\theta \cos\theta - \sin\varphi(H_C \sin\varphi_{\text{NiFe}} \cos\theta + \sigma_{\text{SHE}}$$
$$+ \sigma_{\text{AHE}} \cos^2\varphi_{\text{NiFe}}) - \cos\varphi[(H_x + H_C \cos\varphi_{\text{NiFe}}) \cos\theta$$
$$- \sigma_{\text{AHE}} \cos\varphi_{\text{NiFe}} \sin\varphi_{\text{NiFe}}] = 0, \quad (2a)$$

$$\sin\varphi[-(H_x + H_C \cos\varphi_{\text{NiFe}}) + \sigma_{\text{AHE}} \cos\varphi_{\text{NiFe}} \sin\varphi_{\text{NiFe}} \cos\theta]$$
$$+ \cos\varphi[H_C \sin\varphi_{\text{NiFe}} + (\sigma_{\text{SHE}}$$
$$+ \sigma_{\text{AHE}} \cos^2\varphi_{\text{NiFe}}) \cos\theta] = 0, \quad (2b)$$

$$H_K \sin\theta \cos\theta + \sin\varphi(H_C \cos\theta - \sigma_{\text{SHE}})$$
$$- \cos\varphi(H_x \cos\theta + \sigma_{\text{AHE}} H_x/H_{\text{EB}}) = 0. \quad (3)$$

By setting $H_x = 0$ and $\varphi_{\text{NiFe}} = 270°$ and thus disabling the AHE effect ($\sigma_{\text{AHE}} = 0$), one could easily obtain $\varphi = 90°$ and Eq. (2) was reduced to Eq. (1), as expected.

An interesting case arose as $H_C \ll |H_x| \ll H_{\text{EB}}$. In this case $\cos\varphi_{\text{NiFe}} \approx H_x/H_{\text{EB}}$ and $\sin\varphi_{\text{NiFe}} \approx -1$. Equation (2a) was further reduced to Eq. (3), from which the influence of the ASHE torque could be easily grasped. The second and third term in Eq. (3) depicted the effect of SHE and ASHE torque, respectively. As shown in Figs. 1(b) and 1(c), due to small H_x, $\sigma_{\text{AHE}} \parallel M_{\text{NiFe}}$ was nearly parallel with the y axis. Similar with the orthogonal relations among H_C, σ_{SHE} and EA of Co, H_x and σ_{AHE} were also normal with each other and both perpendicular to the EA, which enabled the ASHE torque to switch the perpendicular magnetization of the Co layer in type-Z mode.

By solving Eq. (2), we obtained the M_z vs σ_{SHE} curve as shown in Fig. 1(e). Here the σ_{AHE}/J_c efficiency was supposed the same as σ_{SHE}/J_c as reported in Ref. [21]. Noteworthy,
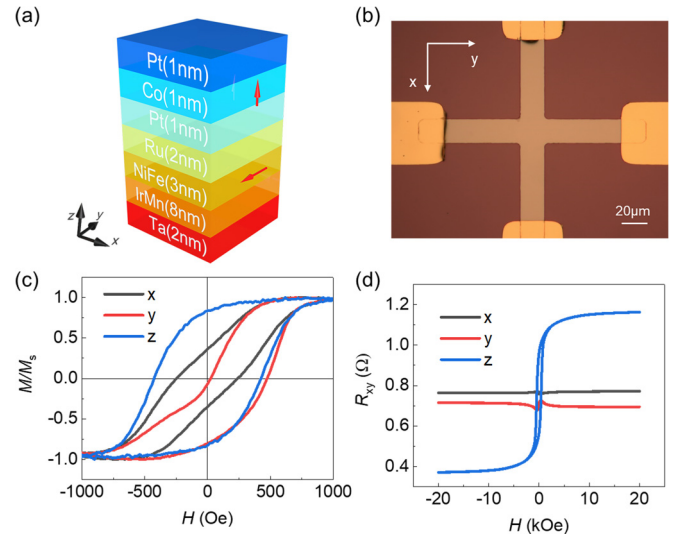

FIG. 2. (a) Stack structure of Ta/IrMn/NiFe/Ru/Pt/Co/Pt, (b) a crossbar device with four terminals, (c) hystereses of the stack measured at different directions, and (d) the dependence of Hall resistance R_{xy} on fields along the three directions. The subfigures (c) and (d) indicate that there existed both perpendicular and in-plane components in the system; (c) also shows an exchange bias H_{EB} of 250 Oe along the y direction.

(1) switching chirality could be changed from clockwise (CW,–1) to counterclockwise (CCW, 1) after the ASHE torque was introduced. (2) Positive and negative H_x resulted in the same M_z vs σ_{SHE}. Comparing Figs. 1(b) and 1(c), $\pm H_x$ made opposite signs for the $M_{\text{NiFe}} \times J_c$ term and as-induced σ_{AHE} were also reversed in sign. As a typical behavior of type-Z switching, simultaneously reversed H_x and σ_{AHE} led to the same final magnetization state, which naturally resulted in the second feature. Figure 1(f) summarizes ΔM_z under different H_x. The sign of ΔM_z indicated chirality of an M_z vs σ_{SHE} curve. As shown by the blue dots and the line in Fig. 1(f), if the ASHE torque was ignored, the sign change could not happen. The above two features were used as a standard to experimentally confirm the ASHE torque in the following.

Figure 2(a) schematically shows the stack structure which was adopted to verify ASHE-torque switching. In this system, the Pt(1)/Co(1)/Pt(1 nm) sandwich was designed to possess PMA. The two Pt layers had the same thickness but were placed on the opposite sides of the Co layer in order to neutralize spin currents of their own. The Ru layer functioned as a coupling spacer, and with this spacer the NiFe could provide an effective in-plane field to the perpendicular Co layer. Under this effective field, the Co layer could be switched by spin-orbit torques from the NiFe in the field-free condition. The 3-nm NiFe was designed as a spin current source. Some pioneering works have already shown a large spin Hall angle in NiFe [23,24,30,31]. Here we went a step further to apply the spin current generated in NiFe to switch magnetization of a perpendicular layer.

The IrMn on the bottom was used to exchange bias the NiFe layer and also increase stability of its in-plane uniaxial anisotropy. Figure 2(b) shows an image of a crossbar device with four terminals. Two of them were used to apply current I
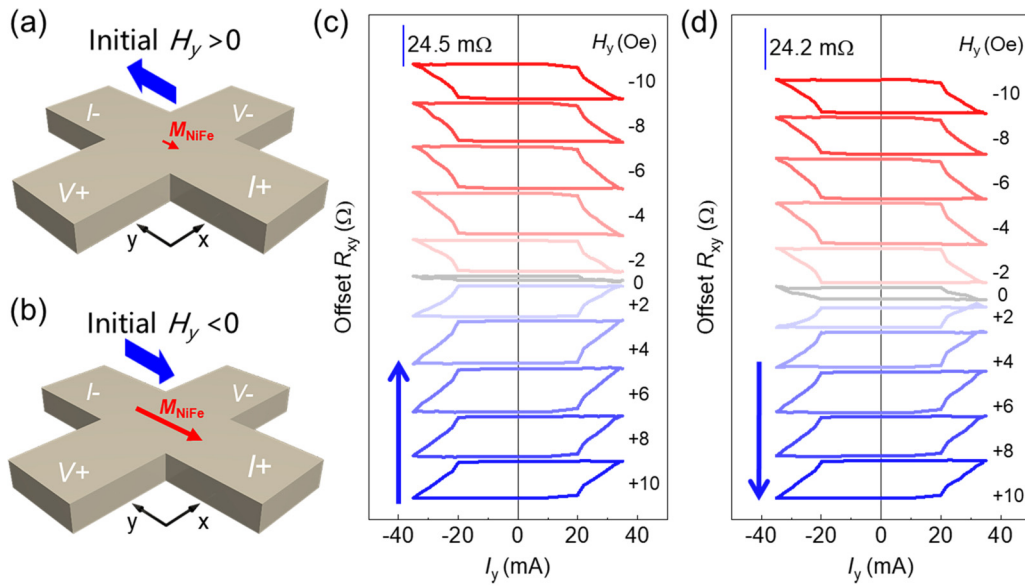
FIG. 3. Measurement setups as reducing H_y to zero from (a) a positive or (b) a negative field. Different initializing processes led to different amounts of M_{NiFe} remanence. (c) SOT switching driven by I_y as H_y set from positive to negative fields. (d) The same measurement but with H_y set from negative to positive values.

along the x or y axis, and the other two picked up Hall voltages V_H along the y or x axis. Then Hall resistance defined as V_H/I was adopted to monitor magnetization m_z of the Co layer via AHE. Since being pinned by the IrMn layer, the relatively thick NiFe layer was hardly rotated by spin-orbit torques when current was applied. Thus, its contribution to the Hall resistance via the planar Hall effect was ignored. Figures 2(c) and 2(d) show hystereses of the full stack via VSM and Hall measurement, respectively. A perpendicular component could be clearly detected by both techniques. Moreover, an exchange bias field H_{EB} of about 250 Oe along the y axis was also observed. This feature would be helpful to field-free switch the above Co layer as shown below.

Next, we used spin-orbit torque of NiFe to switch M_{Co}. Higher (lower) R_{xy} means $M_{z,Co} > 0$ ($M_{z,Co} < 0$). Firstly, we scanned current I_y along the y direction and meanwhile set the external magnetic field H_y at a fixed valve between $+10$ Oe and -10 Oe [Fig. 3(a)]. Larger fields were also tried, which led to the same or reduced switching degree. Here M_{NiFe} was fixed along the y axis. Only SHE instead of ASHE torque played roles [Fig. 1(a)]. As shown in Figs. 3(c) and 3(d), when $I_y > 20$ mA and $H_y > 0$, the spin-up state was favored while the opposite spin-down state was obtained when either direction of I_y or H_y was reversed. H_y determined switching chirality, CW or CCW, as reported before in a type-Z SOT scheme [3,10]. The maximized resistance change ΔR_{xy} due to the SOT switching effect at different H_y was about 24 mΩ. It should be noted that this value was smaller than the $\Delta R_{xy}(H_z = 0)$ value in the H_z dependence of Hall resistance [Fig. 2(d)] because the latter also contained contribution from the tilted NiFe due to interlayer coupling. In contrast, the former ΔR_{xy} was only caused by the reversal of the perpendicular Co layer. Thus, we would use this value as a reference to calculate switching degree in the following part.

We have also tried similar measurement for the Ru/Pt/Co/Pt control sample. However, no switching loops were obtained there, indicating that the IrMn/NiFe layers worked as the dominant SOT source. Considering much higher resistivity of IrMn than NiFe and a short spin diffusion length 2.5 nm of NiFe [32–34], we supposed that spin current absorbed by the Co layer mainly came from the NiFe layer. NiFe has been reported to own sizable spin Hall angles [23,24,30,31], which supported our supposition.

Noticeably, the switching behaviors at $H_y = 0$ depended on magnetizing history due to the exchange-biased NiFe layer. When H_y was reduced to zero from a positive value [Fig. 3(a)] there was little NiFe remanence. The effective field from the NiFe and experienced by the Co therefore tended to zero, which made type-Z switching impossible [Fig. 3(c)]. However, when we reduced H_y to zero from a negative value [Fig. 3(b)], a large NiFe remanence was retained, which assisted the type-Z switching scheme at zero H_y [Fig. 3(d)]. Field-free switching also confirmed magnetic coupling between the NiFe and Co layers. The coupling field H_C was about 1 Oe.

Interestingly, we have applied another setup [Figs. 1(b), 1(c) and Fig. 4(a)] to make ASHE torque play a role. Figure 4 shows switching behaviors when we applied I_y and H_x. First, field-free switching was robustly realized as the NiFe layer was pinned along the y direction. The switching chirality was CW (-1). As the increase in $|H_x|$ rose above a critical value, for example, 5 Oe here, switching chirality was indeed reversed from CW (-1) to CCW (1) [Fig. 4(b)]. ΔR_{xy} was defined as $R_{xy}(I_y = 0, \uparrow) - R_{xy}(0, \downarrow)$ for the CCW loops or $R_{xy}(I_y = 0, \downarrow) - R_{xy}(0, \uparrow)$ for the CW loops. The obtained H_x dependence of ΔR_{xy} was shown in Fig. 4(c). We repeated the measurement 10 times and their ΔR_{xy} results were summarized there as well, confirming the reproducibility of this phenomena. Figure 4(c) had a similar even symmetry
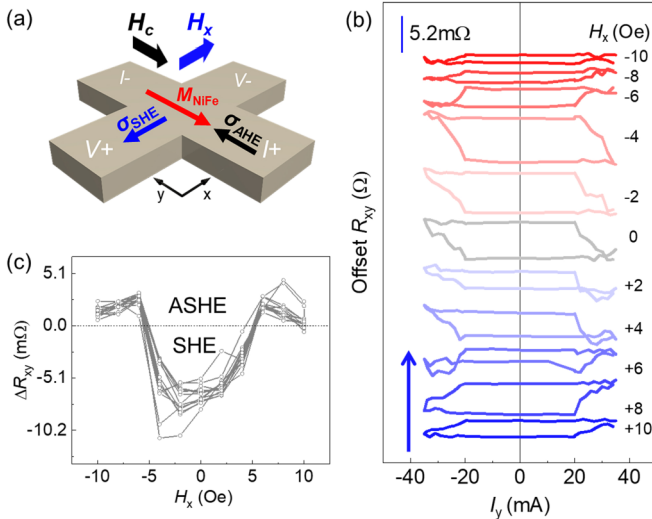
FIG. 4. (a) Measurement setup as applying I_y and H_x. Directions of M_{NiFe}, H_C, σ_{SHE}, and σ_{AHE} are schematically marked. This subfigure depicts a case of small H_x so that M_{NiFe} is nearly aligned along the y axis. (b) Switching behaviors as I_y and H_x applied. (c) H_x dependence of ΔR_{xy} repeated by 10 times. The dotted line separates regions with CW (-1) and CCW ($+1$) switching chirality.

regarding H_x with Fig. 1(e). More crucially, it reproduced the chirality reversal. These behaviors led us to the conclusion that the ASHE torque functioned in this process. Meanwhile this chirality reversal ruled out the possibility that SOT was dominated by IrMn, which should provide σ_{SHE} with fixed polarization.

The H_K of the perpendicular Co layer was about 420 Oe as estimated from the VSM result (Fig. 1). Thus, according to Fig. 4, H_x/H_K was only about $0.014 \sim 0.024$ where the chirality was reversed. However, these values were still in the SHE switching regime according to Fig. 1(f). This discrepancy between experiment and modeling could originate from two reasons. (1) The macrospin model was instructive only in predicting symmetry but inaccurate to give a quantitative prediction on the critical condition for the transition from SHE-dominated to AHE-dominated regimes. (2) Figure 4 shows the switching degree was only about 20% if we used $\Delta R_{xy}(I=0) = 24$ mΩ in Fig. 3(c) as a reference. The small switching degree indicated only some domains with reversed magnetization nucleated. Normally, those nucleation centers had lower anisotropy than the bulk region and thus, magnetization switching started at these centers. Therefore, when comparing Fig. 4 with Fig. 1(f), we needed to use smaller H_K of those nucleation centers instead of the bulk value 420 Oe. Or in other words, H_x/H_K of $0.014 \sim 0.024$ should be an underestimation.

Note that switching by the ASHE and SHE torque in Fig. 4 was partial. Their switching degrees were about 10% and 20%, respectively, compared with $\Delta R_{xy}(I=0) = 24$ mΩ in the R_{xy} vs I_y curve in Fig. 3. This partial switching could possibly be due to the applied H_x and the coupling field H_C being both smaller than the DMI field of the Pt/Co/Pt sandwich [35].

Using the critical switching current density in the ASHE- and SHE-dominated regimes, we roughly estimated the relative magnitudes of the ASHE and SHE angles of NiFe, assuming the current-induced magnetization switching was coherent as a macrospin. In our work, the average critical current for pure SHE-induced magnetization switching was around 27.4 mA, and the average critical current for AHE-dominated magnetization switching was around 26.0 mA. Thus the relative efficiency $\theta_{ASHE}^{NiFe}/\theta_{SHE}^{NiFe}$ was 1.05. This value was comparable to the reported value of 1.28 found in Ref. [34]. Certainly, the estimation was based on the macrospin model. More reliable and accurate methods of calibrating ASHE efficiency in ferromagnets are still to be developed.

We did (not) observe similar behaviors in the devices with $t_{NiFe} = 5$ nm (1 nm), demonstrating that the ASHE torque came from the bulk NiFe instead of its interface with the Ru or IrMn layer. Note that the macrospin model in Fig. 1 could only qualitatively match with the experimental results in Fig. 4 since the macrospin model had no capability to deal with factors such as thermal activation, domain nucleation, and domain wall motion. These factors could all reduce critical current density and make multistate switching practical. A more explicit micromagnetic simulation model taking all the above factors into account would be helpful to interpret the detailed influence of new types of SOTs in the future.

ASHE of ferromagnetic materials can bring about the following advantages for spin-orbitronic devices. (1) The removal of heavy metal such as Pt can help to bring down the cost. (2) AHE- and PHE-induced spin current from magnetic materials has magnetization-controllable polarization, which provides us ways to produce more flexible torques and more versatile performances. (3) Magnetic interaction between the free layer and the fixed layer can be potentially taken advantage of to realize field-free SOT switching as in Refs. [6,16]. In summary, using a ferromagnetic layer as a spin current source can enable one to design low-cost and field-free MRAM with versatile performance [19].

IV. CONCLUSION

In this article we studied spin-orbit torque switching in the Ta/IrMn/NiFe/Ru/Pt/Co/Pt crossbars. The NiFe could not only provide an in-plane coupling field but also serve as a spin current source via the ordinary and anomalous spin Hall effect. Furthermore, spin torques originating from the SHE and ASHE could switch magnetization of the Co layer with opposite chirality. This finding verified the versatile role of ferromagnetic materials in generating spin currents and switching perpendicular magnetization via SHE and AHE mechanisms, which provides a fundamental basis to develop SOT-MRAM or spin logics free of conventional heavy metals.

[1] I. M. Miron, K. Garello, G. Gaudin, P.-J. Zermatten, M. V. Costache, S. Auffret, S. Bandiera, B. Rodmacq, A. Schuhl, and P. Gambardella, Nature (London) **476**, 189 (2011).

[2] L. Q. Liu, C.-F. Pai, Y. Li, H. W. Tseng, D. C. Ralph, and R. A. Buhrman, Science **336**, 555 (2012).

[3] L. Q. Liu, O. J. Lee, T. J. Gudmundsen, D. C. Ralph, and R. A. Buhrman, Phys. Rev. Lett. **109**, 096602 (2012).

[4] C. Wan, X. Zhang, Z. Yuan, C. Fang, W. Kong, Q. Zhang, H. Wu, U. Khan, and X. Han, Adv. Electron. Mater. **3**, 1600282 (2017).

[5] X. Wang, C. Wan, W. Kong, X. Zhang, Y. Xing, C. Fang, B. Tao, W. Yang, L. Huang, H. Wu, M. Irfan, and X. Han, Adv. Mater. **30**, 1801318 (2018).

[6] W. J. Kong, C. H. Wan, X. Wang, B. S. Tao, L. Huang, C. Fang, C. Y. Guo, Y. Guang, M. Irfan, and X. F. Han, Nat. Commun. **10**, 233 (2019).

[7] A. Hoffmann, IEEE Trans. Magn. **49**, 5172 (2013).

[8] J. Sinova, S. O. Valenzuela, J. Wunderlich, C. H. Back, and T. Jungwirth, Rev. Mod. Phys. **87**, 1213 (2015).

[9] J. Kim, J. Sinha, M. Hayashi, M. Yamanouchi, S. Fukami, T. Suzuki, S. Mitani, and H. Ohno, Nat. Mater. **12**, 240 (2013).

[10] X. Zhang, C. H. Wan, Z. H. Yuan, Q. T. Zhang, H. Wu, L. Huang, W. J. Kong, C. Fang, U. Khan, and X. F. Han, Phys. Rev. B **94**, 174434 (2016).

[11] L. Zhu, L. Zhu, M. Sui, D. C. Ralph, and R. A. Buhrman, Sci. Adv. **5**, eaav8025 (2019).

[12] G. Yu, P. Upadhyaya, Y. Fan, J. G. Alzate, W. Jiang, K. L. Wong, S. Takei, S. A. Bender, L.-T. Chang, Y. Jiang *et al.*, Nat. Nanotechnol. **9**, 548 (2014).

[13] C.-F. Pai, L. Liu, Y. Li, H.-W. Tseng, D. C. Ralph, and R. A. Buhrman, Appl. Phys. Lett. **101**, 122404 (2012).

[14] L. J. Zhu, K. Sobotkiewich, X. Ma, X. Li, D. C. Ralph, and R. A. Buhrman, Adv. Funct. Mater. **29**, 1805822 (2019).

[15] S. Fukami, C. Zhang, S. DuttaGupta, A. Kurenkov, and H. Ohno, Nat. Mater. **15**, 535 (2016).

[16] Y.-W. Oh, S.-h. C. Baek, Y. M. Kim, H. Y. Lee, K.-D. Lee, C.-G. Yang, E.-S. Park, K.-S. Lee, K.-W. Kim, G. Go *et al.*, Nat. Nanotechnol. **11**, 878 (2016).

[17] W. J. Kong, Y. R. Ji, X. Zhang, H. Wu, Q. T. Zhang, Z. H. Yuan, C. H. Wan, X. F. Han, T. Yu, K. Fukuda, H. Naganuma, and M.-J. Tung, Appl. Phys. Lett. **109**, 132402 (2016).

[18] Y. Fan, P. Upadhyaya, X. Kou, M. Lang, S. Takei, Z. Wang, J. Tang, L. He, L.-T. Chang, M. Montazeri, G. Yu, W. Jiang, T. Nie, R. N. Schwartz, Y. Tserkovnyak, and K. L. Wang, Nat. Mater. **13**, 699 (2014).

[19] T. Taniguchi, J. Grollier, and M. D. Stiles, Phys. Rev. Appl. **3**, 044001 (2015).

[20] V. P. Amin and M. D. Stiles, Phys. Rev. B **94**, 104419 (2016).

[21] S. Iihama, T. Taniguchi, K. Yakushiji, A. Fukushima, Y. Shiota, S. Tsunegi, R. Hiramatsu, S. Yuasa, Y. Suzuki, and H. Kubota, Nat. Electron. **1**, 120 (2018).

[22] C. Safranski, E. A. Montoya, and I. N. Krivorotov, Nat. Nanotechnol. **14**, 27 (2019).

[23] K. S. Das, J. Liu, B. J. van Wees, and I. J. Vera-Marun, Nano Lett. **18**, 5633 (2018).

[24] S. C. Baek, V. P. Amin, Y. Oh, G. Go, S. J. Lee, G. H. Lee, K. J. Kim, M. D. Stiles, B. G. Park, and K. J. Lee, Nat. Mater. **17**, 509 (2018).

[25] H. Wu, S. A. Razavi, Q. Shao, X. Li, K. L. Wong, Y. Liu, G. Yin, and Kang L. Wang, Phys. Rev. B **99**, 184403 (2019).

[26] T. Seki, S. Iihama, T. Taniguchi, and K. Takanashi, Phys. Rev. B **100**, 144427 (2019).

[27] J. D. Gibbons, D. MacNeill, R. A. Buhrman, and D. C. Ralph, Phys. Rev. Appl. **9**, 064033 (2018).

[28] V. P. Amin, J. Li, M. D. Stiles, and P. M. Haney, Phys. Rev. B **99**, 220405(R) (2019).

[29] S. Fukami, T. Anekawa, C. Zhang, and H. Ohno, Nat. Nanotechnol. **11**, 621 (2016).

[30] H. Wu, C. H. Wan, Z. H. Yuan, X. Zhang, J. Jiang, Q. T. Zhang, Z. C. Wen, and X. F. Han, Phys. Rev. B **92**, 054404 (2015).

[31] W. L. Yang, J. W. Wei, C. H. Wan, Y. W. Xing, Z. R. Yan, X. Wang, C. Fang, C. Y. Guo, G. Q. Yu, and X. F. Han, Phys. Rev. B **101**, 064412 (2020).

[32] V. Tshitoyan, C. Ciccarelli, A. P. Mihai, M. Ali, A. C. Irvine, T. A. Moore, T. Jungwirth, and A. J. Ferguson, Phys. Rev. B **92**, 214406 (2015).

[33] S. Dubois, L. Piraux, J. M. George, K. Ounadjela, J. L. Duvail, and A. Fert, Phys. Rev. B **60**, 477 (1999).

[34] K. S. Das, W. Y. Schoemaker, B. J. van Wees, and I. J. Vera-Marun, Phys. Rev. B **96**, 220408(R) (2017).

[35] C.-F. Pai, M. Mann, A. J. Tan, and G. S. D. Beach, Phys. Rev. B **93**, 144409 (2016).